High-Quality Ultralong Bi_2S_3 Nanowires: Structure, Growth, and Properties

Y. Yu,[†] C. H. Jin,[†] R. H. Wang,[†] Q. Chen,[‡] and L.-M. Peng*,[‡]

Beijing Laboratory of Electron Microscopy, Institute of Physics, Chinese Academy of Science, Beijing 100080, China, and Key Laboratory for the Physics and Chemistry of Nanodevices and Department of Electronics, Peking University, Bejing 100871, China

Received: March 12, 2005; In Final Form: May 10, 2005

A simple one-step hydrothermal method for large-scale synthesis of ultralong single-crystalline Bi_2S_3 nanowires was reported, and the nanowires were comprehensively characterized. The diameters of the nanowires are about 60 nm, and their lengths range from tens of microns to several millimeters. The structure of the nanowires was determined to be of the orthorhombic phase, the growth direction was along [001], and the growth mechanism was investigated based on extensive high-resolution transmission electron microscopy observations. Optical absorption experiments revealed that the Bi_2S_3 nanowires are narrow-band semiconductors with a band gap $E_g \approx 1.33$ eV. Electrical transport measurements on individual nanowires gave a resistivity of about 1.2 Ω cm and an emission current of 3.5 μA at a bias field of 35 V/μm. This current corresponds to a current density of about 10^5 A/cm^2, which makes the Bi_2S_3 nanowire a potential candidate for applications in field-emission electronic devices.

1. Introduction

In recent years, one-dimensional semiconductor nanomaterials, including nanotubes and nanowires, have attracted a wide range of interest because of their remarkable electronic, magnetic, optical, catalytic, and mechanical properties and their potential applications in nanodevices.[1−3] Among these semiconductors, bismuth sulfide is a direct band gap layered semiconductor that crystallizes in the orthorhombic system (*pbnm* space group) and is isostructural to Sb_2S_3 and Sb_2Se_3.[4] The photoconductivity in Bi_2S_3 was reported by Case in 1917 based on studies on mineral samples of bismuthinite or bismuth glance.[5] This ascribes to Bi_2S_3 the status of one of the earliest photoconducting materials known until the early 1920s.[6] Gorinunova et al.[7] studied the conductivity and photoconductivity of some ternary and pseudobinary compounds and, in particular, of Bi_2S_3. From the photoconductivity spectra, they obtained a gap energy of 1.4 eV at room temperature, which is about the optimum band gap for photovoltaic conversion.[7] Bismuth sulfide has also been proposed as a good electrode for liquid-junction solar cells.[8−11] Owing to its good photoconductivity and useful photovoltaic properties, extensive investigations on Bi_2S_3 were carried out in the 1970s and 1980s, especially on thin film prepared by various methods, including chemical depositions,[12−14] evaporation techniques,[10,11] and epitaxial growth.[15] In recent years, many methods have been developed to synthesize one-dimensional bismuth sulfide nanomaterials, including nanotubes,[16] nanoribbons,[17] and nanorods.[18−20] But typically the nanorod products contain some impurities, and their lengths range from several hundred nanometers to several microns. This not only increases the production cost but also makes it more difficult to scale up production. It is therefore highly desirable to develop simple and mild methods for large-scale synthesis of high-quality long nanowires. In this paper, we report a simple hydrothermal method for synthesizing high-purity single-crystal Bi_2S_3 nanowires with lengths up to a few millimeters by reacting with $Bi(NO_3)_3{\cdot}5H_2O$ and $Na_2S{\cdot}9H_2O$ in the solution of tetramethylammonium hydroxide. When $Bi(NO_3)_3{\cdot}5H_2O$ was replaced by $Sb(NO_3)_3$, Sb_2S_3 nanowires with lengths of several microns were obtained. The electrical transport properties of single Bi_2S_3 nanowires have also be investigated in situ inside a transmission electron microscope (TEM); both resistivity and electron field-emission current were measured for individual Bi_2S_3 nanowires.

2. Experimental Section

All chemical reagents used in this experiment were analytical grade. In a typical experiment, 0.0025 mol of $Bi(NO_3)_3{\cdot}5H_2O$ was first added to 60 mL of a tetramethylammonium hydroxide solution (10 wt %) to produce white precipitate. After the solution was stirred for 2 h, 0.00375 mol of $Na_2S{\cdot}9\ H_2O$ was introduced, and the white precipitate turns into black precipitate. The mixed solution was then transferred into a Teflon-lined stainless steel autoclave (80 mL capacity), which was sealed and maintained at 180 °C for 3 days. After the reaction, the resulting black solid products were filtered and washed with distilled water to remove residual ions in the products. The final products were then dried in air.

Powder X-ray diffraction (XRD) experiments were performed with a Rigaku D/max 2400 diffractometer using monochromatic Cu Kα radiation ($\lambda = 1.54$ Å) under 40 kV and 120 mA and scanning between 10° and 70° (2θ). TEM experiments were performed using a Philips Tecnai G20 and a field-emission gun TEM CM200/FEG, both operated at 200 kV. Scanning electron microscopy (SEM) experiments were carried out using a field-emission gun SEM XL30 S-FEG. Composition of the specimens was analyzed using energy-dispersive X-ray (EDX) spectroscopy attached to the Tecnai G20. The specimens for TEM studies were prepared by dispersing the products in alcohol followed by ultrasonic treatment. The sample was then dropped onto a holey carbon film supported on a copper grid and dried in air. Band gap energy of the product was determined from the onset

* Author to whom correspondence should be addressed. E-mail: lmpeng@pku.edu.cn.
[†] Chinese Academy of Science.
[‡] Peking University.

10.1021/jp051294j CCC: $30.25
Published on Web 09/21/2005

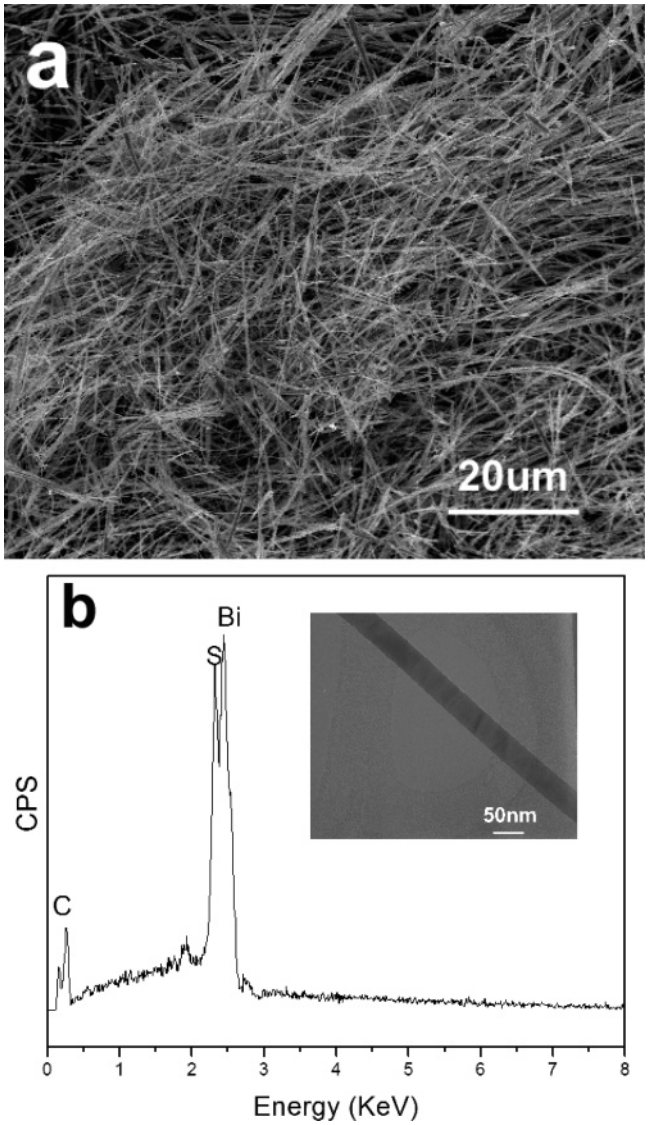

Figure 1. Morphology and composition analysis of the as-synthesized products. (a) SEM image of the products showing the products are high-purity and ultralong nanowires. (b) EDX spectrum taken from a single nanowire giving the nanowires a possible composition of Bi_2S_3. The insert in part b shows a typical nanowire used in EDX experiments.

of the absorbance spectra of the sample using a UV−vis−near-IR spectrophotometer (Shimadzu UV-3100). The electrical transport properties of individual Bi_2S_3 nanowires were investigated inside a Tecnai G20 equipped with a Nanofactory TEM-STM sample holder. The XRD simulations were carried out using Cerius2 software and a SGI 2100 computer workstation.

3. Results and Discussions

Figure 1a is a SEM image of the as-synthesized product showing that the product contains a large quantity of nanowires without any visible byproducts, suggesting that the product is of high quality. The lengths of the nanowires range from tens of microns to a few millimeters. Extensive TEM observations show that the product contains many free-standing nanowires and nanowire bundles and that the nanowires have a narrow size distribution with a diameter around 60 nm. Shown in Figure 1b (the insert) is a single free-standing nanowire having a diameter of about 60 nm. To investigate the shape of the nanowire, a free-standing nanowire was selected and titled along its axis. It was observed that the width of the nanowire hardly

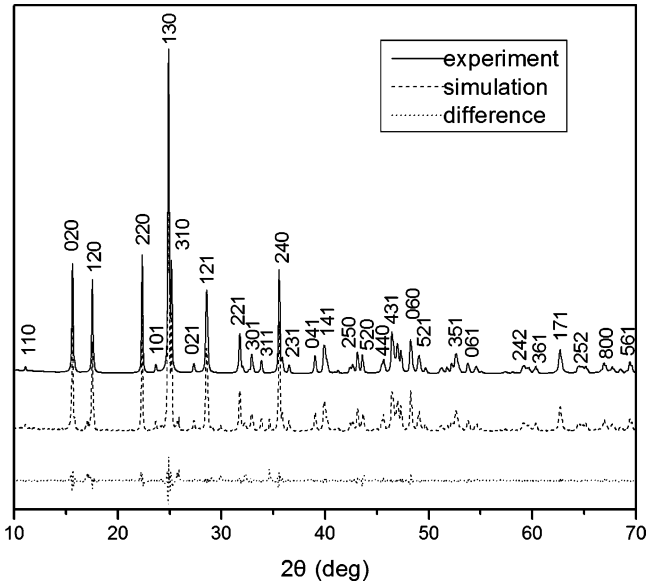

Figure 2. Experimental and simulated XRD profiles. The solid curve is the experimental XRD profile, which may well be indexed using the orthorhombic phase Bi_2S_3 (JCPDS 43-1471), the dashed curve is the simulated profile, and the dotted curve represents the difference between the experimental and the simulated XRD profiles.

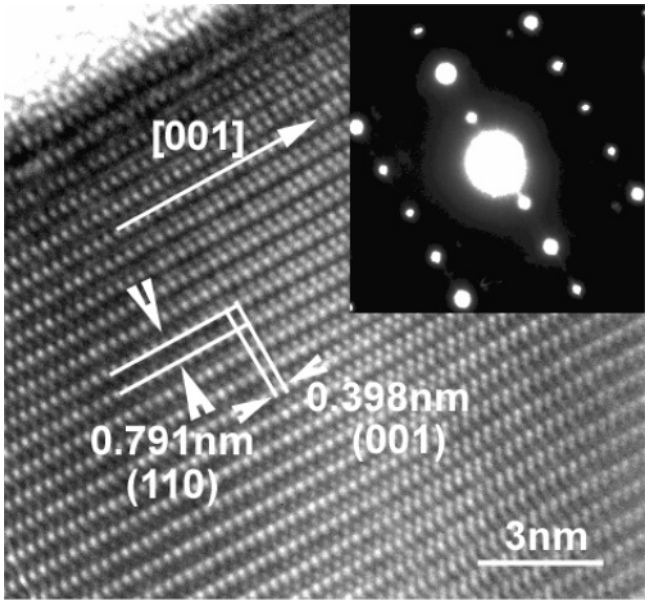

Figure 3. HRTEM image of a typical Bi_2S_3 nanowire. The insert is the corresponding SAED pattern taken along the [1$\bar{1}$0] zone axis.

changed with tilting angles, suggesting that it has approximately a circular cross section perpendicular to its axis. To determine the composition of the nanowires, EDX experiments were performed on individual nanowires. Figure 1b is an EDX spectrum obtained from a single free-standing nanowire as shown in the insert of Figure 1b. Only Bi and S peaks are observed in this spectrum together with the C peak, which was generated by the carbon film on the copper grid, suggesting that the nanowires are composed of mainly Bi and S. Quantitative EDX analysis shows that the atomic ratio of Bi/S is 39:61, close to 2:3, giving a possible composition of Bi_2S_3.

XRD experiments and simulations were carried out to determine the structure of the nanowires, and the results are shown in Figure 2. The solid curve shown in Figure 2 is an experimental XRD profile taken from the nanowire sample showing that all of the peaks may be indexed as the orthor-

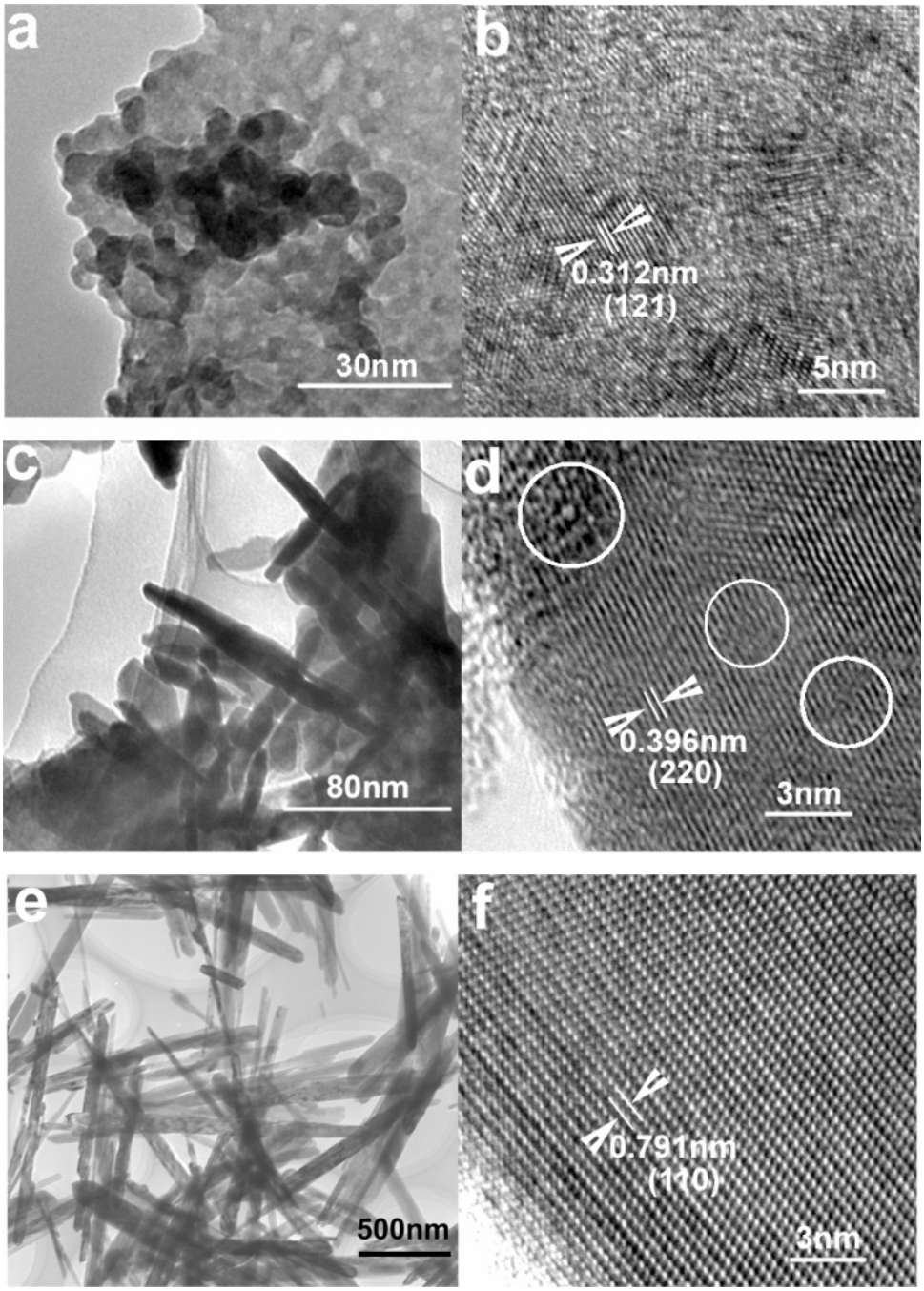

Figure 4. Series of TEM and HRTEM images showing the growth process of the nanowires. Parts a and b show some Bi_2S_3 granular crystals before hydrothermal reaction; parts c and d show that nanorods began to appear after reaction for 3 h; parts e and f show that the nanorods became longer and better-crystallized after 10 h of reaction.

hombic phase Bi_2S_3 (cell constants $a = 11.15$ Å, $b = 11.30$ Å, $c = 3.981$ Å; Joint Committee on Powder Diffraction Standards (JCPDS) Card No. 43-1471). To further test the structure of the Bi_2S_3 nanowire, the XRD data was analyzed with the Rietveld refinement method using the reflex program of MSI, and the results are shown with the dashed curve in Figure 2. The simulation was carried out using the lattice constants given in JCPDS 43-1471, and the simulated XRD profile is seen to agree well with that obtained experimentally. The small difference (dotted curve) between experimental and simulated XRD profiles suggests that our nanowire sample is of a very high-purity single-phase sample.

Shown in Figure 3 is a high-resolution transmission electron microscopy (HRTEM) image and the corresponding selected area electron diffraction (SAED). Like the XRD profile, the HRTEM image and the SAED pattern may also be indexed using the orthorhombic phase of Bi_2S_3 (JCPDS 43-1471). The observed lattice spacings of 0.79 and 0.398 nm correspond to the (110) and (001) planes of the orthorhombic Bi_2S_3, respectively. The SAED pattern taken along the $[1\bar{1}0]$ zone axis reveals that the nanowire is single-crystalline in nature. Both the HRTEM image and the SAED pattern show that the nanowires grew along the [001] direction. The growth direction coincides with that reported for Bi_2S_3 nanorods but not for Bi_2S_3 nanoribbons.[17]

To understand the growth process, extensive TEM observations were made on samples with different hydrothermal reaction times, and the results are shown in Figure 4. In a typical experiment, $Bi(NO_3)_3$ was first strongly hydrolyzed in the tetramethylammonium hydroxide solution to produce white

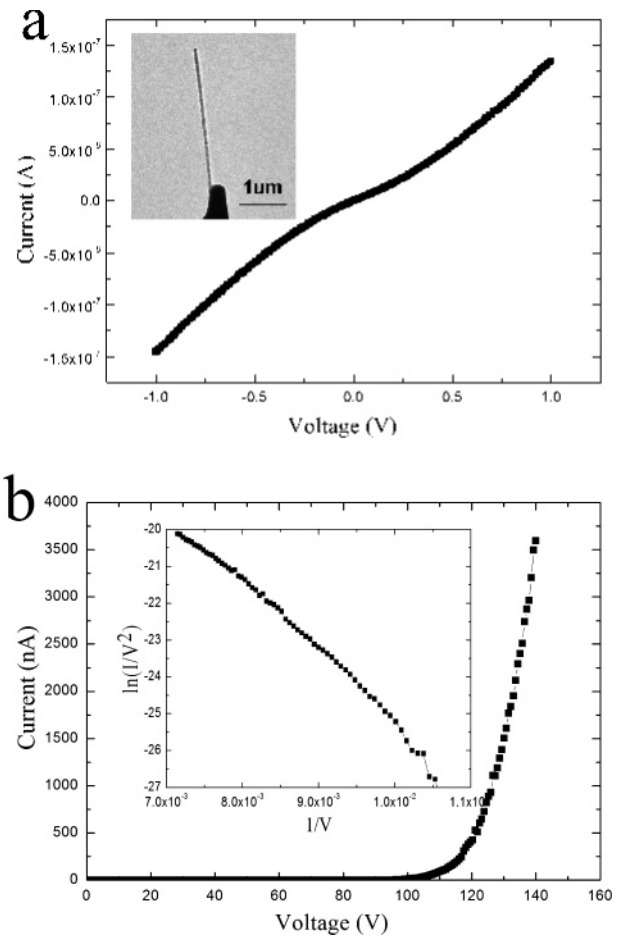

Figure 5. Electrical transport measurements on Bi_2S_3 nanowires. (a) Two-terminal $I-V$ curve recorded in situ inside a TEM at room temperature. The insert is a TEM image showing the corresponding Bi_2S_3 nanowire used in the experiment. (b) $I-V$ characteristics of the field-emission measurement performed on the same nanowire as shown in the insert of part a. Inset in part b shows the corresponding Fowler−Nordheim plot of the $I-V$ curve, i.e., $\ln(I/V^2)$ versus $(1/V)$.

precipitate of $BiONO_3$. Once S^{2-} ions were introduced, black precipitate was formed. Figure 4a is a low-magnification TEM image of the black precipitates before hydrothermal treatment showing that the sample consists of granular crystals having sizes between 3 and 5 nm. Figure 4b is a HRTEM image of the same sample showing lattice spacings that are the same as that of orthorhombic phase Bi_2S_3, verifying that these black precipitates are indeed Bi_2S_3 particles. Because Bi_2S_3 has a far smaller solubility than $BiONO_3$ does, $BiONO_3$ is unstable in the hydrothermal condition, and the reaction may therefore proceed spontaneously. After hydrothermal treatment for 3 h, many short nanorods formed about 10 nm in diameter and 60−100 nm in length as shown in Figure 4c. The higher-magnification TEM image shown in Figure 4d reveals that the structure of the short nanorods is the same as that of Bi_2S_3. We concluded therefore that the nanowires grew from merging Bi_2S_3 particles of Figures 4a and 4b. Figure 4d shows that the quality of these short nanorods is rather poor. They are highly disordered and not fully crystallized as marked with circles. Longer reaction times subsequently reduced the disordered and amorphous phase, giving much better quality nanowires. Shown in Figures. 4e and 4f are similar TEM images for longer nanorods obtained from samples after 10 h of hydrothermal reaction. The nanorods shown in Figures 4e and 4f obviously have a better quality than those shown in Figures 4c and 4d. It was also found that during the growth process of the nanowires Bi_2S_3 grows in a preferential direction, i.e., along the [001] direction, and this may be attributed to its inherent chain-type structure.[21]

To understand the role of the tetramethylammonium hydroxide solution on the growth of the nanowires, the tetramethylammonium hydroxide solution was replaced by deionized water. It was found that the samples prior to hydrothermal reaction consisted also of granular crystals of Bi_2S_3 but having much larger diameters of about 60−100 nm. After hydrothermal treatment for 3 days, the final product contained mainly larger particles and short rods, suggesting that the tetramethylammonium hydroxide solution might act effectively as a kind of stabilizer, which controlled the size of the Bi_2S_3 particles and prevented the Bi_2S_3 particles from aggregating into larger ones. On the basis of our experiments, we propose the following three relevant chemical reactions for the growth process of the Bi_2S_3 nanowires:

$$Bi(NO_3)_3 + H_2O \leftrightarrow 2HNO_3 + BiONO_3 \quad \text{(a)}$$

$$2BiONO_3 + 3S^{2-} + H_2O \leftrightarrow Bi_2S_3 + 4OH^- + 2NO_3^- \quad \text{(b)}$$

$$nBi_2S_3 \leftrightarrow Bi_2S_3 \text{ nanowires} \quad \text{(c)}$$

Optical absorption experiments were carried out to elucidate information on the band gap energy, which is one of the most important electronic parameters for semiconductor nanowires. The spectra obtained from our Bi_2S_3 nanowires show a λ_{onset} at about 960 nm. Through the use of the formula given in our previous work,[22] we estimate the band gap $E_g \approx 1.33$ eV, i.e., the nanowires are narrow-band-gap semiconductors.

The electronic transport properties of individual Bi_2S_3 nanowires were investigated inside our TEM using a Nanofactory TEM-STM sample holder.[23] An individual Bi_2S_3 nanowire was attached to the electrochemically etched W tips by spot-welding or electron-induced deposition of amorphous carbon. A typical TEM image of the W tip/nanowire system is shown in the insert of Figure 5a, and another mechanically cut Pt wire (not shown) was used as the counter electrode above this figure. Figure 5a shows a two-terminal current−voltage ($I-V$) curve obtained from the Bi_2S_3 nanowire. Although the $I-V$ curve is not perfectly linear, the resistance of the semiconducting nanowire may be obtained at large bias via dV/dI as shown in ref 24 because the metal/semiconducting contacts affect mainly the low-bias region and the voltage dependence of the total current is determined mainly by the intrinsic resistance of the nanowire at large bias. This procedure gives a resistivity of about 1.2 Ω cm, which is somehow higher than that of a film sample.[25]

After the two-terminal resistance measurements, the nanowire was retracted from the top Pt electrode to leave a gap between the nanowire and the Pt electrode by the moving the W tip for electron field-emission experiments. The field-emission curve from the Bi_2S_3 nanowires with $d = 4$ μm is shown in Figure 5b, with d being the distance between electrondes for field emission. The emitted electron current increased to 10 nA at a threshold voltage of 104 V or initial field of 26 V/μm. The emission current reached 3.5 μA at a field of 35 V/μm, giving a current density of about 10^5 A/cm. Higher current density is expected for smaller vacuum gap d, but too small of a distance may lead to discharge and breakdown of the nanowire. Through the use of Fowler−Nordheim theory, we may write the field-emission current as[26]

$$I = A\frac{1.5 \times 10^{-6}}{\phi}\left(\frac{V}{d}\right)\gamma^2 \exp\left(-\frac{6.44 \times 10^9 \phi^{1.5} d}{\gamma V}\right)$$

where A is the area, γ is the field enhancement factor, and ϕ is the work function in electronvolts. A and γ could be determined from the slope of the $\ln(I/V^2)-1/V$ curve or Fowler−Nordheim plot that depends on d, ϕ, and γ. Following the procedure described in ref 27, we obtained a nominal work function of 5.8 eV for a single Bi_2S_3 nanowire, and this value is close to that for the bulk material of 5.3 eV.[28] Since d is known in our experiments, we can easily get the field enhancement factor $\phi = 200$. It must be emphasized, however, that the Fowler−Nordheim formula was derived for a semi-infinite bulk sample and direct application to nanostructures may lead to a large error. The work function and field enhancement factors given here should be regarded as phenomenological rather than real physical quantities.

4. Conclusions

High-purity Bi_2S_3 nanowires about 60 nm in diameter and up to a few millimeters in length were synthesized by directly reacting with $Bi(NO_3)_3 \cdot 5H_2O$ and $Na_2S \cdot 9\ H_2O$ in tetramethylammonium hydroxide solution. Comprehensive characterizations using XRD, EDX, HRTEM, SAED, and computer simulations show that the nanowires are of the orthorhombic phase Bi_2S_3 (JCPDS 43-1471) and grow along the [001] direction. UV−vis absorption spectra revealed that the nanowires are narrow-band-gap semiconductors with $E_g \approx 1.33$ eV. Electrical experiments on a single nanowire showed that the nominal resistivity of the nanowire is about 1.2 Ω cm, its work function is about 5.8 eV, and the electron field-emission initial field is about 26 V/μm. The electron field-emission current reached 3.5 μA at a bias field of 35 V/μm, giving a current density of about 10^5 A/cm^2.

Acknowledgment. The authors are grateful for the support of the Ministry of Science and Technology (Grant No. 001CB610502), the National Science Foundation of China (Grant Nos. 90206201 and 10434010), the Chinese Ministry of Education (Key Project, Grant No. 10401), and the National Center for Nanoscience and Technology of China.

References and Notes

(1) Huang, Y.; Duan, X. F.; Cui, Y.; Lauhon, L. J.; Kim, K. H.; Lieber, C. M. *Science* **2001**, *294*, 1313.

(2) Bachtold, A.; Hadley, P.; Nakanishi, T.; Dekker, C. *Science* **2001**, *294*, 1317.

(3) Martel, R.; Schmidt, T.; Shea, H. R.; Hertel, T.; Avouris, P. *Appl. Phys. Lett.* **1998**, *73*, 2447.

(4) Hofmann, W. *Z. Kristallogr.* **1933**, *86*, 225.

(5) Case, T. W. *Phys. Rev.* **1917**, *9*, 305.

(6) Bube, R. H. *Photoconductivity in Solids*; Wiley: New York, 1960.

(7) Goriunova, N. A.; Kolomiets, B. T.; Mal'kova, A. A. *Sov. Phys. Technol. Phys.* **1956**, *1*, 1583.

(8) Hodes, G.; Manassen, J.; Cahen, D. *Nature* **1976**, *261*, 403.

(9) Miller, B.; Heller, A. *Nature* **1976**, *262*, 680.

(10) Krishna, P. A.; Shivakumar, G. K. *Thin Solid Films* **1984**, *121*, 151.

(11) Krishna, P. A. *J. Mater. Sci. Lett.* **1984**, *3*, 837.

(12) Pramanik, P.; Bhattacharya, R. N. *J. Electrochem. Soc.* **1980**, *127*, 2087.

(13) Baranski, A. S.; Fawcett, W. R. *J. Electrochem. Soc.* **1980**, *127*, 766.

(14) Baranski, A. S.; Fawcett, W. R.; Gilbert, C. M. *J. Electrochem. Soc.* **1983**, *130*, 2433.

(15) Poliakov, S. M.; Laverko, E. N.; Lisker, I. S.; Pukshanskii, A. A.; Yagodkin, V. M. *Sov. Phys. Solid State* **1975**, *16*, 386.

(16) Ye, C. H.; Meng, G. W.; Jiang Z.; Wang, Y. H.; Wang, G. Z.; Zhang, L. D. *J. Am. Chem. Soc.* **2002**, *124*, 15180.

(17) Liu, Z. P.; Peng, S.; Xie, Q.; Hu, Z. K.; Yang, Y.; Zhang, S. Y.; Qian, Y. T. *Adv. Mater.* **2003**, *15*, 936.

(18) Shen, G. Z.; Chen, D.; Tang, K. B.; Li, F. Q.; Qian, Y. T. *Chem. Phys. Lett.* **2003**, *370*, 334.

(19) Zhang, H.; Ji, Y. J.; Ma, X. Y.; Xu, J.; Yang, D. R. *Nanotechnology* **2003**, *14*, 974.

(20) Wang, H.; Zhu, J. J.; Zhu, J. M.; Chen, H. Y. *J. Phys. Chem. B* **2002**, *106*, 3848.

(21) Boudjouk, P.; Remington, M. P., Jr.; Grier, D. G.; Jarabek, B. R.; Mcarth, G. J. *Inorg. Chem.* **1998**, *37*, 3538.

(22) Du, G. H.; Chen, Q.; Han, P. D.; Yu, Y.; Peng, L.-M. *Phys. Rev. B* **2003**, *67*, 035323.

(23) Jin, C. H.; Wang, J. Y.; Wang, M. S.; Su, J.; Peng, L.-M. *Carbon* **2005**, *43*, 1026.

(24) Zhang, Z. Y.; Jin, C. H.; Liang, X. L.; Chen, Q.; Peng L.-M. Unpublished work.

(25) Chen, B. X.; Uher, C.; Iordanidis, L.; Kanatzidis, M. G. *Chem. Mater.* **1997**, *9*, 1655.

(26) Gadzuk, J. W.; Plummer, E. W. *Rev. Mod. Phys.* **1973**, *45*, 487.

(27) Bai, X. D.; Wang, E. G.; Gao, P. X.; Wang, Z. L. *Nano Lett.* **2003**, *3*, 1147.

(28) Garifullin, M. M.; Zubenko, Y. V.; Yagodkin, V. M. *Radio Eng. Electron. Phys.* **1976**, *21*, 145.